Chapter 2

FOCUSING ON MOVING TARGETS THROUGH SCATTERING SAMPLES

This chapter is adapted from the manuscript Zhou, E.H., Ruan, H., Yang, C. & Judkewitz, B. "Focusing on moving targets through scattering samples". Optica 1, 227 (2014). The contributions of authors are as follows: BJ and CY conceived the initial idea. EHZ and BJ developed the idea and scheme demonstration. The experiments were designed and performed by EHZ and BJ. The data analyses were performed by EHZ, HR, CY, and BJ.

Focusing light through scattering media is of great importance for imaging and stimulation in biomedical optics. While wavefront shaping and optical time-reversal techniques can in principle be used to focus light across scattering media, achieving this within a scattering medium with a noninvasive and efficient reference beacon, or guide star, remains an important challenge. In this chapter, we show optical time-reversal focusing using a new technique termed Time Reversal by Analysis of Changing wavefronts from Kinetic targets (TRACK). By taking the difference between time-varying scattering fields caused by a moving object and applying optical time reversal, light can be focused back to the location previously occupied by the object. We demonstrate this approach with discretely moved objects as well as with particles in an aqueous flow, and obtain a focal peak-to-background strength of 204 in our demonstration experiments. We further demonstrate that the generated focus can be used to noninvasively count particles in a flow-cytometry configuration—even when the particles are hidden behind a strong diffuser. By achieving optical time reversal and focusing noninvasively without any external guide stars, using just the intrinsic characteristics of the sample, this work paves the way to a range of scattering media imaging applications, including underwater and atmospheric focusing as well as noninvasive *in vivo* flow cytometry.

2.1 Introduction

Focusing light through highly scattering media is an important challenge in biomedical imaging, colloidal optics, and astronomy. When light propagates through strongly scattering samples, refractive index inhomogeneities scatter the light field in many directions. This was long thought of as a randomizing process, which

precludes the formation of a sharp focus. However, by taking advantage of the deterministic nature of scattering, researchers in the field of complex wavefront shaping have demonstrated that light can be focused at an arbitrary location within and across scattering media—by shaping the input wavefront reaching the sample [1, 2]. Because appropriate input wavefronts are complex and because they depend on sample structure as well as target location, determining them remains a key challenge. With direct optical access to the input plane and the focusing plane, wavefronts can be found with one of three strategies: iterative optimization [1, 3–5], optical time reversal[6], or measuring and inverting the sample transmission matrix [7, 8]. When there is no direct access to the target plane, e.g., when the target plane is hidden within the sample, physical guide stars such as beads can be placed within the sample and used as reference beacons [9–11]. Because this requires invasive insertion, recent research has focused on virtual, ultrasound-based guide stars relying on the acousto-optic [12–16] or the photo-acoustic effect[17–20]. However, all of these strategies are either limited by the acoustic resolution (tens of micrometers at best) or require many measurements, thereby increasing the recording time by orders of magnitude. Thus far, near-instantaneous time reversal at optical resolutions remains elusive. Here we introduce a new all-optical method, termed Time Reversal by Analysis of Changing wavefronts from Kinetic targets (TRACK), which achieves precise optical time reversal to a target hidden behind a scattering sample—without the need for acoustic guide stars. Unlike previous techniques, this method uses the motion of the target itself to serve as a guide star.

2.2 Principles

A concise setup for noninvasively focusing light through a scattering sample is shown in Fig. 2.1. The complete setup can be found in the latter section. We interpret optical scattering through our diffuser as a linear process described by a complex spatial transmission matrix, $T(x_a, x_b)$ [1]. This matrix defines the transformation of the optical field at an input plane with coordinates x_a directly before the diffuser to an output plane with coordinates x_b behind the diffuser, where we have a moving target with a reflectivity function $R(x_b)$. We assume that our digital phase-conjugation system is set up such that we can discretely measure and control the optical field along the input plane coordinates x_a.

Our detect-and-refocus process is composed of four primary steps. First, we illuminate the scatterer with an input wave, $U(x_a)$, to reflect light off our target. $U(x_a)$ transforms into a speckle field at the output plane as defined by the transmission

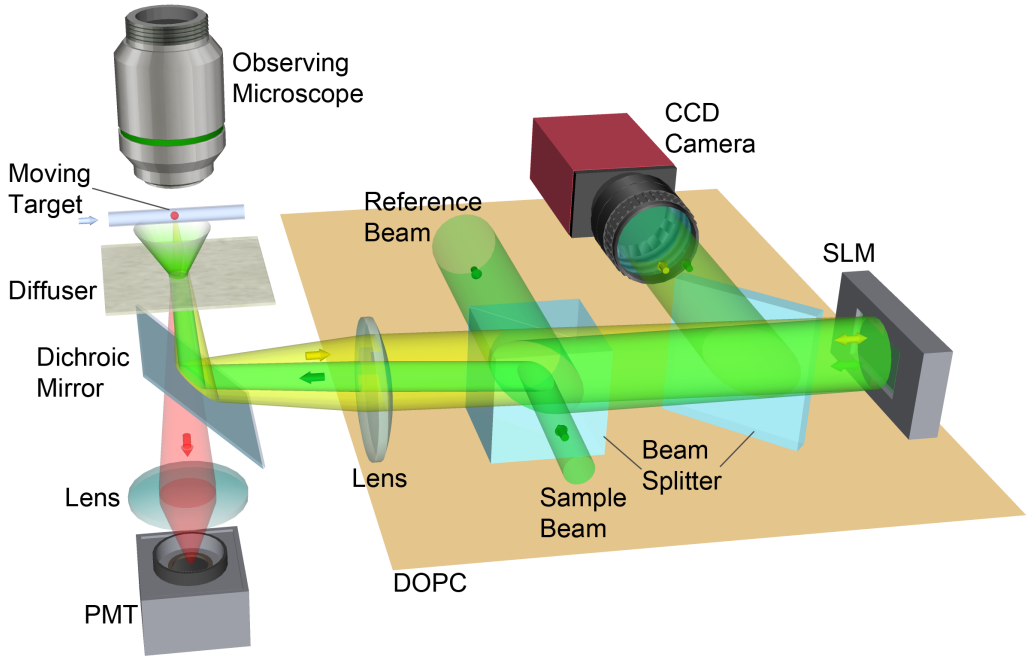

Figure 2.1: **Concise setup including sample for TRACK**: varying backscattered wavefronts due to a target's movement are captured by off-axis holography. The phase of the wavefront difference is time reversed by the digital optical phase-conjugation (DOPC) system. Diffuse light is focused back to the previous position of the target.

matrix: $S(x_b) = T(x_a, x_b)U(x_a)$. A portion of the speckle field $S(x_b)$ will hit our target object with reflectivity function $R(x_b)$. The target object's back-reflected optical field is thus the product $E_1(x_b) = R(x_b)S(x_b)$. Note that $R(x_b) = 0$ and hence $E_1(x_b) = 0$ everywhere except along the target's finite spatial extent. We also assume $S(x_b) \neq 0$ somewhere along our target to ensure a nonzero reflected signal.

Second, we measure the entire backscattered optical field at the input plane, $M_1(x_a)$, as depicted in Fig. 2.2(a). Following linear optics, we split the backscattered field $M_1(x_a)$ into a sum of two components: one reflected from out target object at the output plane, $E_1'(x_a)$, and one originating from all other locations within the sample volume, $B(x_a)$. The target-dependent component $E_1'(x_a)$ is defined as the target-reflected optical field at the output plane, $E_1'(x_b)$. After it has backscattered to the input plane. Following the common assumption of a lossless scattering process, we may use our transmission matrix to express $E_1'(x_a)$ as

$$E_1'(x_a) = T^t(x_a, x_b)E_1(x_b), \tag{2.2.1}$$

where T^t, the transpose of T, represents the reverse process of scattering from the output to the input plane. The total measured field at the input plane is thus the sum

$$M_1(x_a) = T^t(x_a, x_b)E_1(x_b) + B(x_a), \tag{2.2.2}$$

where again $B(x_a)$ is the background optical field arising from all other locations within the sample.

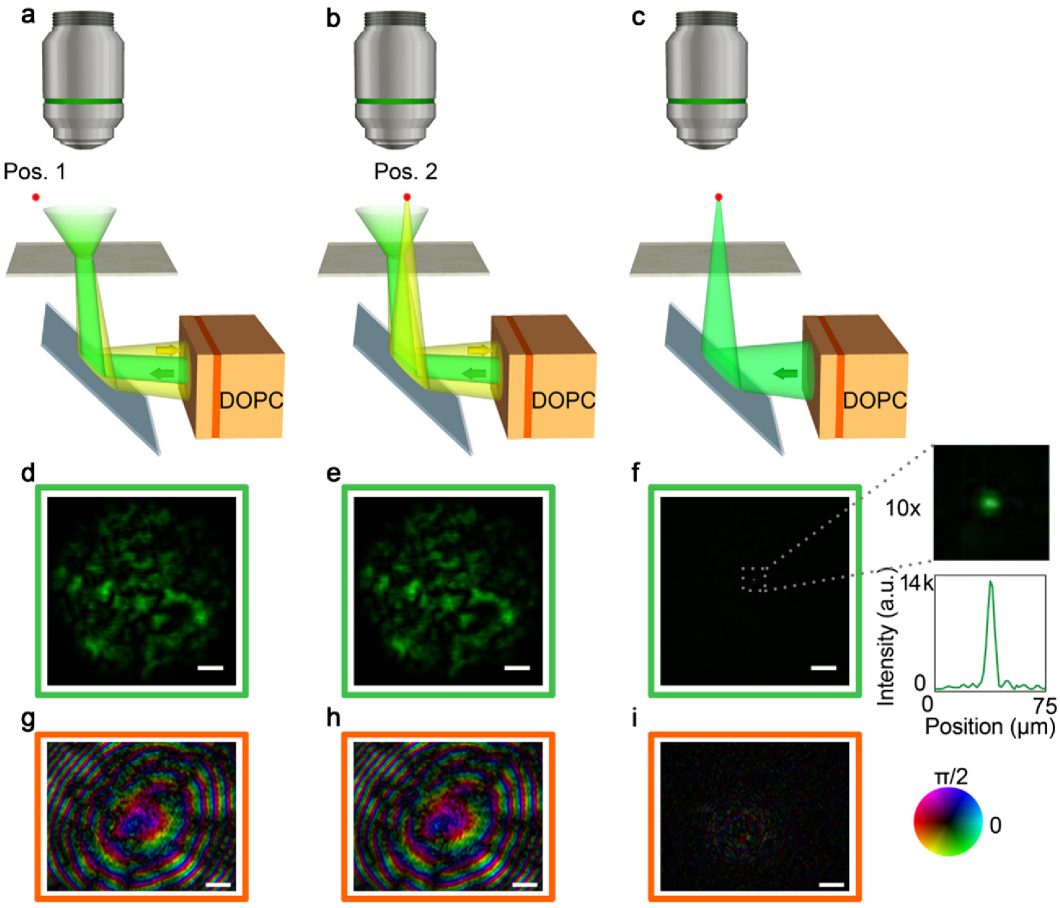

Figure 2.2: **Focusing on a moving target through a scattering sample**: (a) target at position 1 (far off the illuminated field of view); (b) target at position 2 (within the illuminated field of view); (c) light is focused behind the diffuser; (d)–(f) corresponding images recorded with the observing microscope; (g) and (h) phase maps recorded at the camera imaging the SLM surface; (i) difference of field in (g) and field in (h). The cross-section intensity distribution in (f) indicates a PBR of 204. Scale bars in (d)–(f) are 100 μm. Scale bars in (g)–(i) all stand for 1 mm.

Third, we measure a second backscattered field at the input plane, $M_2(x_a)$, after the reflective target object physically shifts a finite distance Δ across the output plane. This measurement is depicted in Fig. 2.2(b). A spatially shifted target will generate

a new reflected field, $E_2(x_b) = R(x_b - \Delta)S(x_b)$, which will again transform to the input plane via our transmission matrix and combine with a background field contribution to yield

$$M_2(x_a) = T^t(x_a, x_b)E_2(x_b) + B(x_a). \tag{2.2.3}$$

Equation 2.2.3 implicitly assumes that T and $B(x_a)$ remain the same as for the first measurement, requiring the scattering sample to be stationary (apart from target motion) at the time scale of the measurement interval.

Fourth, we digitally subtract our two measurements to efficiently remove and background contribution and isolate the target-reflected signal:

$$M_2(x_a) - M_1(x_a) = T^t(x_a, x_b)[E_2(x_b) - E_1(x_b)]. \tag{2.2.4}$$

We compute the phase conjugate of this subtraction and display it on our digital optical phase-conjugation (DOPC) setup's spatial light modulator (SLM) to create the following field at the input plane: $T^\dagger[E_2(x_b) - E_1(x_b)]^*$, where $\dagger$ denotes a conjugate transpose and $*$ a complex conjugation. This field scatters from the sample's input to output plane to form our final target-focused field, $E_f(x_b)$, as shown in Fig. 2.2(c):

$$E_f(x_b) = T(x_a, x_b)T^\dagger(x_a, x_b)[E_2(x_b) - E_1(x_b)]^* \approx [E_2(x_b) - E_1(x_b)]^*. \tag{2.2.5}$$

Here, we assume a complete scattering process to form the approximation $T(x_a, x_b)T^\dagger(x_a, x_b) \approx I$, the identity matrix. Conjugate light thus forms the field $E_2 - E_1$ at the sample plane, implying light is focused to both shifted target positions. If the target was originally off the laser speckle field (i.e., E_1 is zero everywhere), a focus will appear only at its second location, which corresponds to our ability to refocus onto a moving object.

2.3 Methods

Setup

All data were collected by a self-built optical system schematically described in Fig. 2.3. In the setup, we used a 532 nm fiber-coupled semiconductor laser (Spectra Physics, Excelsior 532). The polarization of the beam was made horizontal (by a half-wave plate and polarizing beam splitter), which is in accordance with SLM (Holoeye, PLUTO) modulation polarization. Beam splitter 1 splits the incoming light into two beams: the sample beam and the reference beam. The sample beam

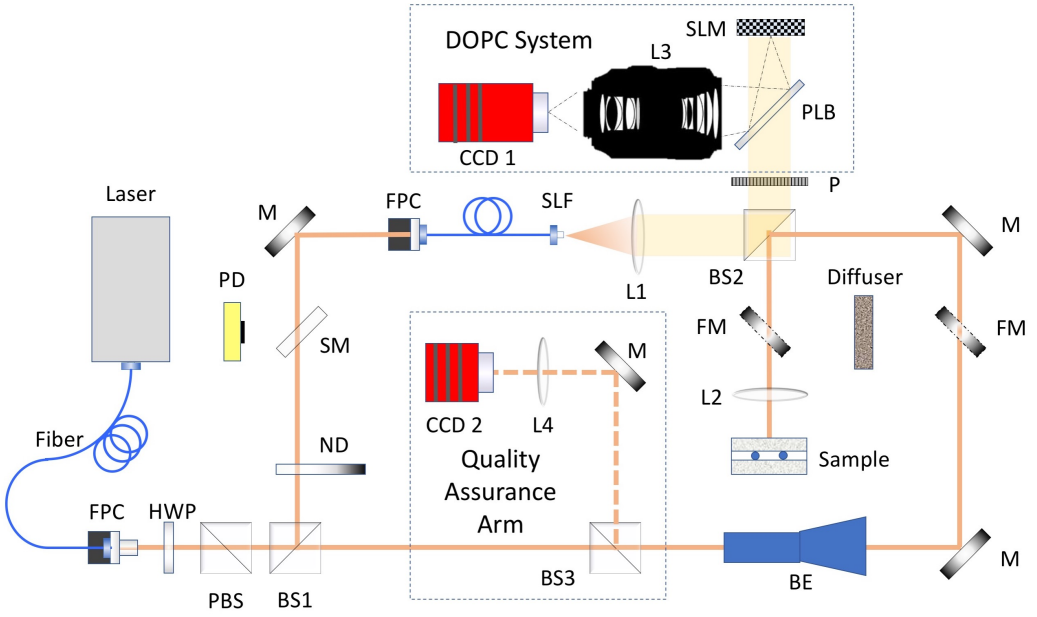

Figure 2.3: **Full setup diagram for TRACK**: Abbreviation: ND-Neutral Density filter wheel, BE-Beam Expander, BS1,2,3-Beam Splitter 1,2,3, BSH-Beam shutter, D-Diffuser, FM-Flip Mirror, FPC-Fiber Port Collimator, HWP-Half wave Plate,L1,2,3-Lens 1,2,3, M-Mirror, P-Polarization Plate, PBS-Polarizing Beam Splitter, PD-Photo Detector, PLB-Plate beam splitter, SM-Sample Mirror, SLF-Spatial Light Filter, SLM-Spatial Light Modulator.

was expanded by a laser expander for a suitable size of laser spot at the sample. Reflected by mirrors and beam splitter 2, the sample beam passed through lens 2 and was eventually reflected to the sample by a dichroic mirror, which was at a 45° angle to the horizontal plane (it is hard to show in the 2D scheme in Fig. 2.3; details of the sample setup can be found in Fig. 2.1). The sample was placed close to the focal plane of lens 2. Light backscattered by the sample was collected to the SLM by lens 2. The reference beam passed through a neutral density filter and was coupled into a single-mode polarization maintaining fiber for spatial filtering. After exiting the fiber, the beam was collimated by lens 1. Scattered light and reference light were combined by beam splitter 2 before reaching the DOPC system. Polystyrene beads were obtained from Life Technology. Retro-reflective beads, which consisted of aluminum coated 50 µm glass spheres, were obtained from Cospheric. To create samples we used adhesive backed, highly diffusing films (3M Scotch model no.810, 60 µm thick), which did not transmit a detectable ballistic component (measured with a detection threshold of 10^{-8} of the illumination power).

We used it as a random phase plate diffuser whose angle scattering distribution is plotted in appendix. To show that our results can be extended to biological samples, we performed TRACK experiments through a 0.5 mm thick section of *ex vivo* chicken muscle tissue (scattering coefficient μ_s: 30 mm^{-1} and anisotropy parameter g: 0.965 [14]). The results of this experiment are shown in appendix.

Fluorescence Signal Capture

In the flow-cytometry experiment, we used orange fluorescent (540/560) polystyrene microspheres obtained from Life Technology. As shown in Fig. 2.6(c), orange fluorescence from the beads propagated through the diffuser along with diffuse backscattered light at 532 nm. Colors were separated by the dichroic mirror (a 532 edge pass filter, model Di02-R532-25 $\times$ 36 from Semrock). Underneath the dichroic mirror, a lens images the surface of the diffuser to a compact PMT. The fluorescence spectrum of the sample and the transmission spectrum of edge pass filter are shown in Fig. 2.4. A median filter was used to filter the signal shown in Fig. 2.6(e).

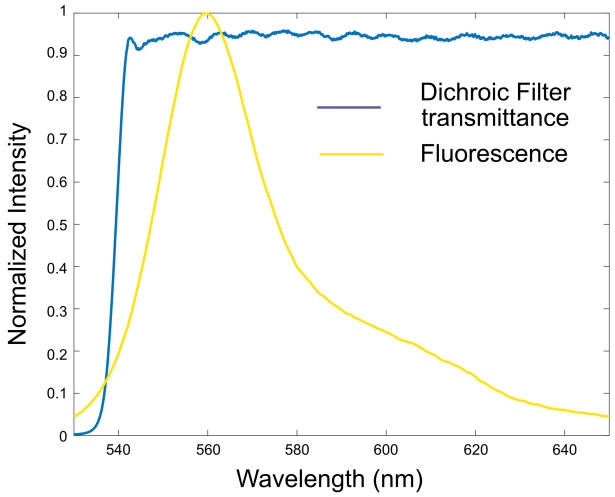

Figure 2.4: **Fluorescence spectrum of cytometry bead and dichroic mirror transmission spectrum.**

Reference Phase Correction

As aforementioned in discussion, in digital phase conjugation, reference beam and SLM curvature will affect the conjugate phase map and thus the time-reversal PBR. By digitally modulating the SLM curvature to iteratively maximize the reflection

from the SLM back into the single-mode fiber in the reference beam arm, we can compensate for SLM curvature as well as reference beam phase errors [14]. A threefold enhancement is observed.

Quality Assurance Setup

To assure the pixel-to-pixel alignment between the camera and SLM and the performance of the DOPC system, a quality assurance arm was configured in the sample arm including two flipping mirrors, beam splitter 3, a mirror, lens 4 and camera 2 (as shown in Fig. 2.3). When flip mirrors were flipped up, the system was changed from the reflective mode to the transmission mode. When applying time reversal, we expected to observe a focus on camera 2. By tuning the position and tilting of the SLM, we optimized the intensity of the focus. In this way, a day-to-day precise alignment of the DOPC system was guaranteed.

2.4 Results

Direct Observation of Optical Focusing in Reflection Mode

Our reflection-mode TRACK setup is diagramed in Fig. 2.1. To record backscattered light at the SLM plane, a camera was pixel-to-pixel aligned to image the SLM surface, and wavefronts were measured by off-axis holography [21, 22]. For demonstration, we created a sample consisting of 10 μm diameter polystyrene beads behind a highly diffusing tape. The beads were placed on a glass slide 7 mm behind the diffuser, whose movement was two-dimensionally controlled by a piezo stage. To confirm the formation of a focus through scattering media, an observing microscope (OM) was set up to image the target plane from the back. Importantly, this microscope was only used for validation of successful focusing, but not to derive wavefronts or create the foci.

We started by recording a backscattered wavefront without any targets behind the diffuser (Fig. 2.2(g)) and compared it to the wavefront measured when a target was inside the illuminated field of view (Fig. 2.2(h)). As expected, both wavefronts were dominated by backscattering from the entire diffuser, while the relative difference of the wavefronts was 15% (relative average amplitude) [Fig. 2.2(i)]. When we time reversed the difference wavefront by digital phase conjugation, the OM recorded a high-contrast focus at the location of the target. Fig. 2.2(f) includes a plot of the intensity profile (horizontal section across the peak), which shows a peak-to-background ratio (PBR) of 204.

Moving Target Tracking behind Scattering Media

If we keep repeating this experiment with a continuously moving target, light will be focused dynamically on the target. In other words, we can track the moving target through the scattering medium. To confirm this experimentally, we recorded a background wavefront at the SLM plane (with no target bead in the illuminated area), and subsequently moved a target bead to multiple locations within the illuminated area. At each position of the target [as shown in Figs. 2.5(a)–(c)], after recording the wavefront, we subtracted the background wavefront from the current wavefront and time reversed the result such that it focused on the current location of the target [as shown in Figs. 2.5(d)–(f)]. A detailed timing diagram of the system is included in the appendix. In this experiment, a 50 µm diameter retro-reflective target bead was 14 mm behind the diffuser.

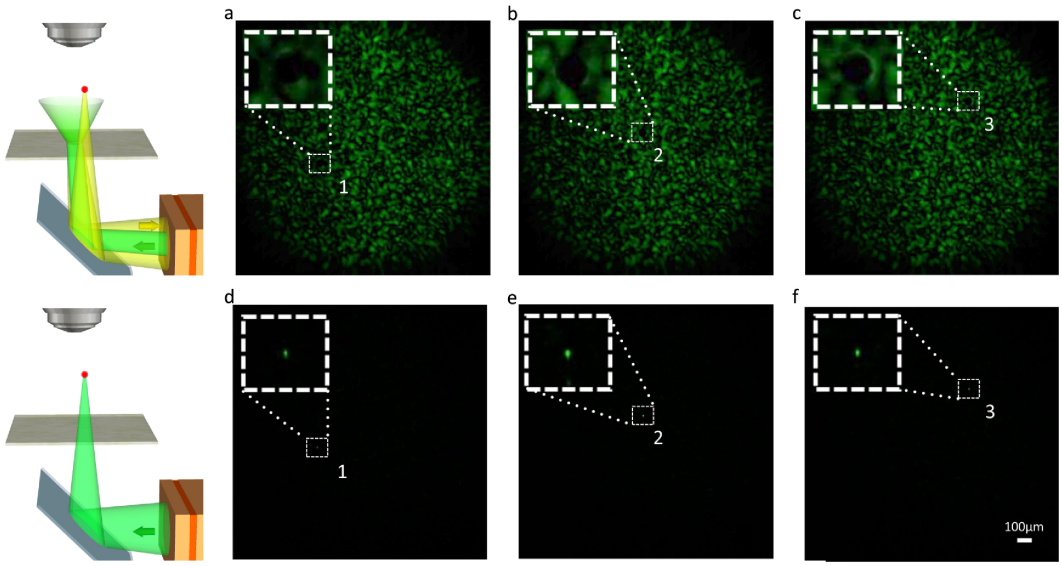

Figure 2.5: **Target tracking by TRACK**: images taken with the observing microscope. (a)–(c) Images of targets at positions 1–3 in the laser speckle; (d)–(f) phase conjugate foci at corresponding positions.

Optical Flow Cytometry in Scattering Media

To mimic an in vivo flow-cytometry scenario, we placed a microfluidic channel behind the diffuser. Two kinds of beads were used in this experiment: nonfluorescent polystyrene beads as guide stars and fluorescent beads to be counted in a flowcytometry-type setup. Repeating the first experiment ("direct observation of optical focusing," above) in a microfluidic channel, we recorded two scattering fields with a guide star bead outside and inside the illuminated area (Fig. 2.6(a)

and Media 1). We then phase conjugated the difference wavefront and observed a focus at the exact position of the guide bead (as shown in Fig. 2.6(c) and Media 1). From the cross-section intensity distribution, we measured a PBR of 134 and a full width half-maximum (FWHM) of 8.9 µm. After formation of the focus, fluorescence beads were flown at a speed of 5 cm/s, and the time-varying fluorescence signal was recorded by a single-channel photomultiplier tube (PMT). The PMT trace contained clearly detectable signals that corresponded to fluorescent beads passing the focus. Illumination, phase conjugation, and fluorescence detection by the PMT all occurred on the same side of the scattering sample in a reflection geometry.

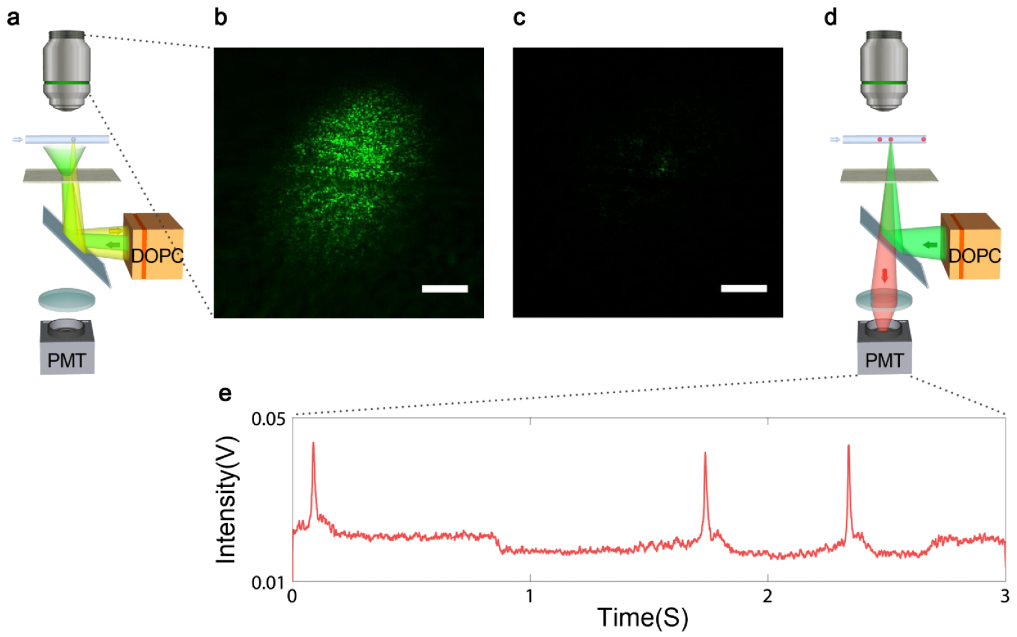

Figure 2.6: **Optical flow cytometry in scattering media**: (a) schematic of the recording step, in which a focus is established as above; (b) laser speckle shining on the microfluidic channel as imaged by the observing camera; (c) time-reversed focus established with the help of the first bead; (d) schematic of the particle counting setup; (e) signal captured on the PMT with clear signals caused by fluorescent beads passing the focus. Both scale bars stand for 100 µm.

2.5 Discussion

In this work we provided, to the best of our knowledge, the first demonstration of time-reversed optical focusing through scattering media by using the motion of a target object as a guide star—a technique we call TRACK. We would like to use this section to note some points of consideration associated with this work.

First, TRACK will focus on all backscattering targets that moved between the two

wavefront recordings. If the goal is to focus on a single target or bead, only one moving backscattering bead should be within the illuminated area.

Second, we would like to point out that our experimental setup associated with the experimental findings shown in Fig. 2.2,2.5 and 2.6 contain a microscope objective and camera (outlined in green in 2.1) that allowed us to directly observe the space after the diffuser. We used that imaging system to directly observe and verify that the TRACK focus was achieved. In practical applications, it is unlikely that such an observation perspective would be available. In most of the application scenarios, our only access to the target of interest would be on one side of the diffusing medium, in a reflection geometry. A good case in point would be the task of reflection-mode focusing of light through skin and into a blood vessel. The reflection-mode focusing results presented here show that focusing light in this geometry is feasible. For example, upon creating the time-reversed optical focus (Fig. 2.6), we can observe the passage of fluorescent beads through the microfluidic channel by simply observing the upticks in fluorescence scattered back through the diffuser. Another important trade-off space this method introduces is an intrinsic relationship between focus spot size and achievable PBR. Mathematically, these two quantities are related to each other through the number of optical modes that the DOPC can capture and control during playback [23]:

$$PBR_{phase-only} \approx \frac{\pi}{4} \cdot \frac{N_{SLM}}{N_{target}}, \tag{2.5.1}$$

where N_{SLM} indicates modes on the SLM from the scattering of the target and N_{target} represents the number of modes modulated by the target in the speckle plane. The above formula contains a $\pi/4$ factor because the DOPC in this set of experiments is a phase-only modulator system. For the experimental setup used for Fig. 2.2, the above formula predicts a focus PBR of 390—a quantity that is consistent with our experimental result of 204, indicating a time-reversal efficiency of >50%. The above formula leads to an interesting consequence. By using smaller target objects, we can effectively create a tighter optical focus and simultaneously boost the PBR. However, we caution that the use of ever smaller target objects will lead to a weaker initial scattering signal arriving at the DOPC and in turn degrade the time-reversed wavefront in the presence of noise. This will then reduce the focus PBR.

As the different sets of experimental results reported in Figs. 2.5 and 2.6 show, this method can be used to create a time-reversed focus that tracks with the target object or to create a fixed and static focus at a specific location along the trajectory of the object. Each of these focusing types is useful for different applications: dynamic

tracking can potentially be useful for following moving targets in deep ocean or convective atmosphere environments, while the static focus would be most useful for flow-cytometry-type applications.

Appendix

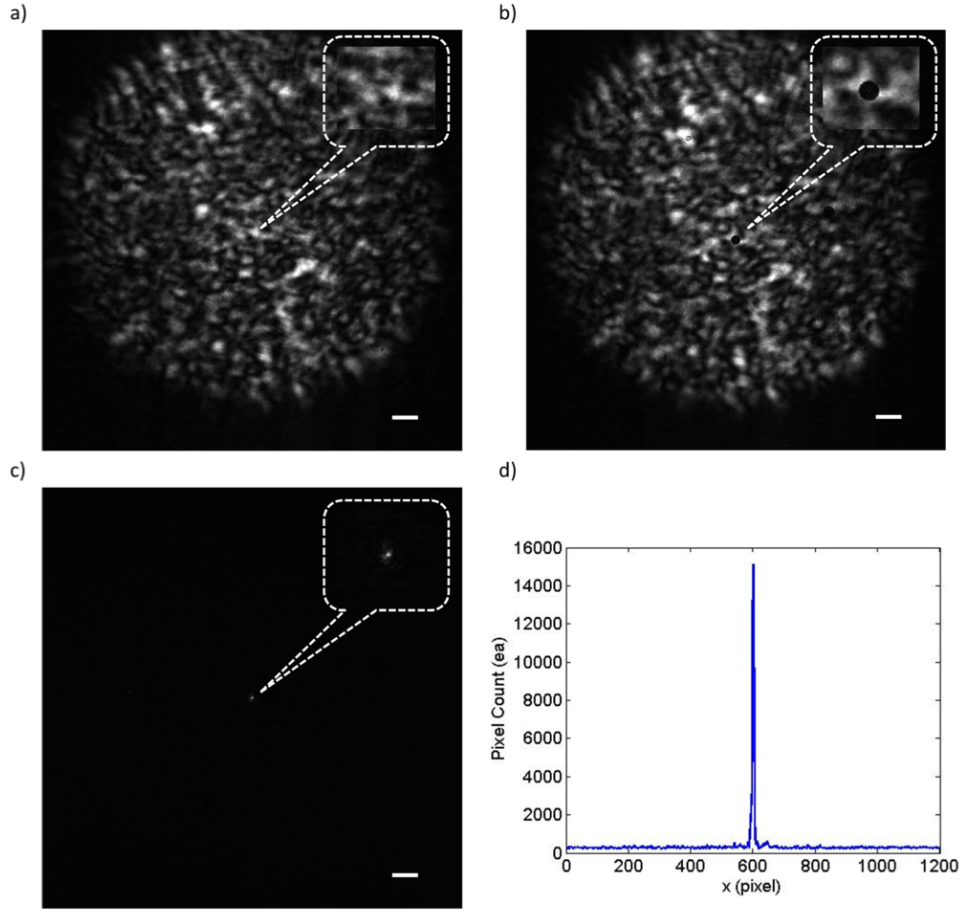

Figure 2.7: TRACK focusing with an experimental setup analogous to the one in Fig. 2.2, except that the diffuser was replaced with 0.5 mm thick chicken breast tissue (μ_s: 30 mm^{-1}). a) Laser speckle captured when the target is outside the speckle formed behind a 0.5 mm thick section of chicken breast. b) Laser speckle when the target moves in. c) Phase-conjugate focus. d) Cross section of the focus. Scale bars: 100 µm.

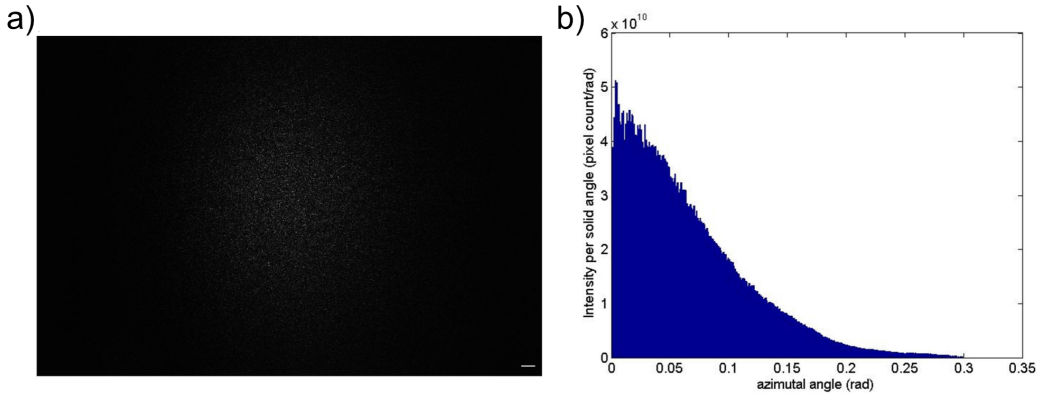

Figure 2.8: **Angle distribution of the diffusing sample**: a) Speckle pattern captured 7.25cm behind the diffuser attached to a pinhole shined laser through. b) Distribution of intensity scattering angle. Scale bar: 1 mm.

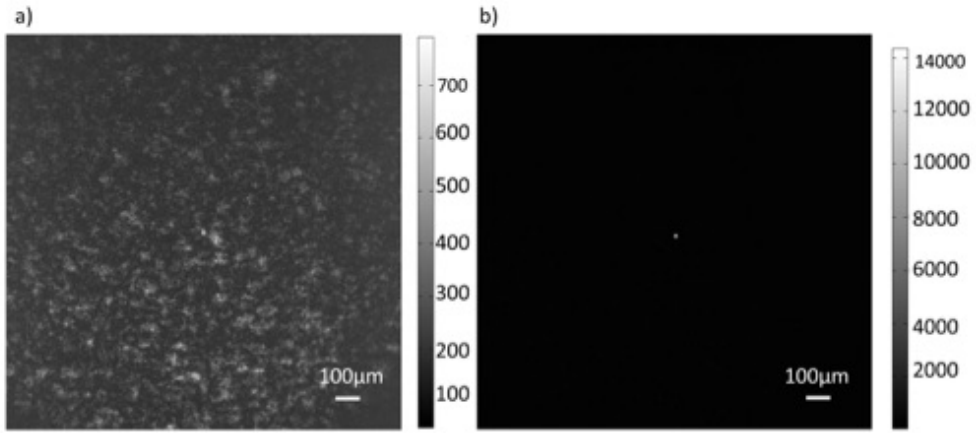

Figure 2.9: To compare TRACK to traditional reflective bead guide-stars, we performed an experiment analogous to the one described in Fig. 2.2, but started by time-reversing just one wavefront M_1 (recorded when a reflective bead was present behind the scattering medium – see Eq. 2.2.2. a) Image recorded by the observing camera when such a wavefront was time-reversed. The focus is barely visible on top of the background. b) TRACK focusing with the difference wavefront $M_1 - M_2$, where M_2 was the wavefront recorded after the target was moved outside the field of view.

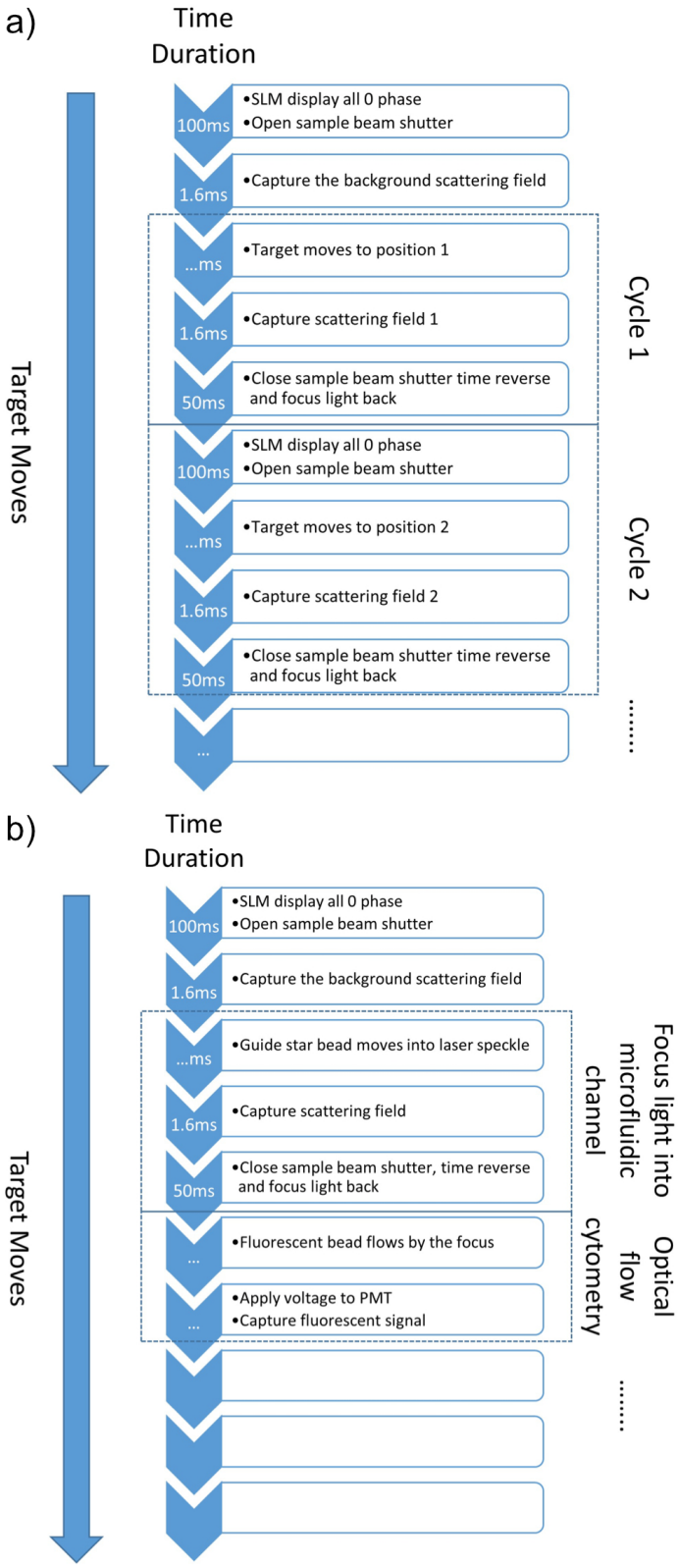

Figure 2.10: **Timing for the experiments**: a) Experiment in Fig. 2.5. b) Experiment in Fig.2.6.

References

[1] Ivo M Vellekoop and AP Mosk. “Focusing coherent light through opaque strongly scattering media”. In: *Optics letters* 32.16 (2007), pp. 2309–2311.

[2] Allard P Mosk et al. “Controlling waves in space and time for imaging and focusing in complex media”. In: *Nature photonics* 6.5 (2012), pp. 283–292.

[3] IM Vellekoop, Ad Lagendijk, and AP Mosk. “Exploiting disorder for perfect focusing”. In: *arXiv preprint arXiv:0910.0873* (2009).

[4] Donald B Conkey, Antonio M Caravaca-Aguirre, and Rafael Piestun. “High-speed focusing of light through dynamic turbid media”. In: *Computational Optical Sensing and Imaging*. Optical Society of America. 2012, CTu4B–6.

[5] Zahid Yaqoob et al. “Optical phase conjugation for turbidity suppression in biological samples”. In: *Nature photonics* 2.2 (2008), pp. 110–115.

[6] Hasan Yılmaz, Willem L Vos, and Allard P Mosk. “Optimal control of light propagation through multiple-scattering media in the presence of noise”. In: *Biomedical optics express* 4.9 (2013), pp. 1759–1768.

[7] SM Popoff et al. “Image transmission through an opaque material”. In: *arXiv preprint arXiv:1005.0532* (2010).

[8] Youngwoon Choi et al. “Scanner-free and wide-field endoscopic imaging by using a single multimode optical fiber”. In: *Physical review letters* 109.20 (2012), p. 203901.

[9] Chia-Lung Hsieh et al. “Digital phase conjugation of second harmonic radiation emitted by nanoparticles in turbid media”. In: *Optics express* 18.12 (2010), pp. 12283–12290.

[10] Ivo M Vellekoop, Meng Cui, and Changhuei Yang. “Digital optical phase conjugation of fluorescence in turbid tissue”. In: *Applied physics letters* 101.8 (2012), p. 081108.

[11] Xiaodong Tao et al. “Live imaging using adaptive optics with fluorescent protein guide-stars”. In: *Optics express* 20.14 (2012), pp. 15969–15982.

[12] Xiao Xu, Honglin Liu, and Lihong V Wang. “Time-reversed ultrasonically encoded optical focusing into scattering media”. In: *Nature photonics* 5.3 (2011), pp. 154–157.

[13] Puxiang Lai et al. “Reflection-mode time-reversed ultrasonically encoded optical focusing into turbid media”. In: *Journal of Biomedical Optics* 16.8 (2011), pp. 080505–080505.

[14] Ying Min Wang et al. “Deep-tissue focal fluorescence imaging with digitally time-reversed ultrasound-encoded light”. In: *Nature communications* 3 (2012), p. 928.

[15] Ke Si, Reto Fiolka, and Meng Cui. “Fluorescence imaging beyond the ballistic regime by ultrasound-pulse-guided digital phase conjugation”. In: *Nature photonics* 6.10 (2012), pp. 657–661.

[16] Benjamin Judkewitz et al. “Speckle-scale focusing in the diffusive regime with time reversal of variance-encoded light (TROVE)”. In: *Nature photonics* 7.4 (2013), pp. 300–305.

[17] Fanting Kong et al. “Photoacoustic-guided convergence of light through optically diffusive media”. In: *Optics letters* 36.11 (2011), pp. 2053–2055.

[18] Donald B Conkey et al. “Super-resolution photoacoustic imaging through a scattering wall”. In: *Nature communications* 6 (2015).

[19] Puxiang Lai et al. “Nonlinear photoacoustic wavefront shaping (PAWS) for single speckle-grain optical focusing in scattering media”. In: *arXiv preprint arXiv:1402.0816* (2014).

[20] Thomas Chaigne et al. “Controlling light in scattering media non-invasively using the photoacoustic transmission matrix”. In: *Nature Photonics* 8.1 (2014), pp. 58–64.

[21] Ulf Schnars and Werner Jüptner. “Direct recording of holograms by a CCD target and numerical reconstruction”. In: *Applied optics* 33.2 (1994), pp. 179–181.

[22] Etienne Cuche, Pierre Marquet, and Christian Depeursinge. “Spatial filtering for zero-order and twin-image elimination in digital off-axis holography”. In: *Applied optics* 39.23 (2000), pp. 4070–4075.

[23] Ivo Micha Vellekoop. “Controlling the propagation of light in disordered scattering media”. In: *arXiv preprint arXiv:0807.1087* (2008).